CrossMark

ARTICLE

Morphology evolution and visible light driven photocatalysis study of Ti^{3+} self-doped TiO_{2-x} nanocrystals

Fang Li and Tiehu Han
Department of Chemistry, Zhejiang Sci-Tech University, Hangzhou 310018, China

Huigang Wang[a),b)] and Xuming Zheng[b)]
Department of Chemistry and the Engineering Research Center for Eco-dyeing and Finishing of Textiles, Zhejiang Sci-Tech University, Hangzhou 310018, China

Junmin Wan
Engineering Research Center for Eco-dyeing and Finishing of Textiles, Zhejiang Sci-Tech University, Hangzhou 310018, China

Bukuo Ni
Department of Chemistry, Texas A&M University–Commerce, Commerce, Texas 75429, USA

(Received 15 November 2016; accepted 23 January 2017)

One conceptually different approach has been developed to synthesize Ti^{3+} self-doped TiO_{2-x} mesocrystals to narrow the band gap of TiO_2. This simple and economical one-pot solvothermal method uses $TiCl_3$ and tetrabutyltitanate (TBT) as a precursor and exhibits practical application. Different morphology including uniform spindle shape, tetragonal bipyramid, and capsule-like mesocrystals can be tailored easily by tuning the precursor ratio of $TiCl_3$ to TBT. We have shown that our band gap engineered TiO_{2-x} exhibits unique mesocrystal phase and owns substantial high visible light driven photocatalytic activities. Electron paramagnetic resonance (EPR) studies of this sample verified the presence of oxygen centered radicals, namely, hydroxyl (·OH) and superoxide radicals (O_2^{-}·/·OOH). The catalysts have been characterized using transmission electron microscope, fluorescence spectra, Raman spectra, EPR, X-ray photoelectron spectroscopy, X-ray diffraction (XRD), Ultraviolet–visible absorption spectra, etc. It shows high catalytic stability. The findings of this work provide new insights for developing morphology tailored for visible light driven devices and other applications via controlled band gap engineering.

I. INTRODUCTION

Since Fujishima and Honda reported the first photoelectrochemical cell in 1972 using TiO_2 as a photoanode, great efforts have been exerted on a semiconductor cell for water splitting and photocatalysis in dye degradation.[1] TiO_2 also boasts for its merit of nontoxicity, abundance, superior photocatalytic activity, and long-term chemical stability.[2] But its characteristic of a large band gap and quick recombination of photo-generated electron–hole pairs impede its practical applications.[3] Therefore, pure TiO_2 is not a good candidate; band gap engineering is needed if we want to use TiO_2 as a higher efficiency catalyst under visible light illumination.[4–6]

To date, many approaches have been tried to improve the visible light absorption and prolong the electron–hole pairs' separation lifetime.[3,7,8] Doping with heteroelements is one of the effective methods to tackle these challenges. Cations such as Rh^{3+}, Mo^{4+}, Os^{3+}, Re^{5+}, V^{4+}, Mn^{3+}, and Fe^{3+} were used as dopants to introduce mid-gap electronic states into the TiO_2 forbidden band gap.[9–12] Non-metallic doping such as B/TiO_2[13,14], C/TiO_2[13,15–17], N/TiO_2[13,18,19], S/TiO_2[17,20], F/TiO_2[18,21–23] were also tried. However, the introduction of heteroelements often enhanced the possibility of charge recombination and thermal instability. Recently, appealing approaches based on dopant-free, Ti^{3+} species self-doping in TiO_2 have emerged as an effective approach to overcome this limitation.[24–32]

Several methods have been introduced to produce Ti^{3+} self-doped TiO_{2-x}.[24–27,33] The thermal reducing (CO or H_2) treatment of TiO_2 is a usual method to create Ti^{3+} on its surface to improve the surface and photoelectrochemical properties.[24–27] Physical methods of high energy particle bombardment (such as laser,[34,35] electron,[36] or Ar^{+}[37]) are alternatives to produce Ti^{3+} species in TiO_2. However these methods were all limited by high cost and difficult in large scale production, in addition, Ti^{3+} created using these methods mainly scattered on the surface region and is not thermally stable enough in air or air saturated water solution.[33] Additionally, theoretical

Contributing Editor: Xiaobo Chen
[a)]Address all correspondence to this author.
e-mail: zdwhg@163.com, huigwang@uni-osnabrueck.de
[b)]These authors contributed equally to this work.
DOI: 10.1557/jmr.2017.49

 © Materials Research Society 2017

https://doi.org/10.1557/jmr.2017.49 Published online by Cambridge University Press

calculation demonstrated that only under high Ti^{3+} doping concentration can it form a continuous vacancy mid-gap band of electronic states[24] and a low Ti^{3+} doping concentration on the contrary creates localized oxygen vacancy states that actually play as e–h pair combination sites and deteriorate the visible photoactivity.[38,39] Therefore methodology of high-concentration Ti^{3+} doping with low cost and volume production strategy should be developed to obtain bulk Ti^{3+} self-doped TiO_{2-x}.

Recently, one oxidation-based method using TiH_2 and H_2O_2 as starting materials has been reported to produce Ti^{3+} self-doped TiO_{2-x}. It exhibits higher photocatalytic activity for photooxidation of methylene blue (MB).[33]

In contrast to the above briefed method, we demonstrate herein a one-pot solvothermal method to produce Ti^{3+} self-doped TiO_{2-x} mesocrystals with various tailored morphology. Mesocrystals are the assemblies of crystallographically oriented nanocrystals that were regarded as a new class of ordered nanoparticles.[40] We use $TiCl_3$ and tetrabutyltitanate (TBT) as the starting materials, under solvothermal conditions, $TiCl_3$, and tetrabutyltitanate hydrolysis individually in the acetic acid environment and then calcine at 400 °C to produce homogeneously distributed Ti^{3+} self-doped TiO_{2-x} mesocrystals. This is a simple and cost-efficient process.

II. EXPERIMENTAL SECTION

A. Synthesis of Ti^{3+} self-doped TiO_{2-x}

Ti^{3+} self-doped TiO_{2-x} nanoparticles were prepared by a solvothermal method using $TiCl_3$ and tetrabutyltitanate (TBT) as a precursor. Mix TBT and $TiCl_3$ in a volume ratio of 5:0, 4:1, 3:2, 1:4, and 0:5 individually. In a typical preparation procedure, 1 mL of the above mixture was added into 50 mL acetic acid under vigorous stirring. The suspension was continuously stirred for 30 min at room temperature. After that, the resulting mixtures were transferred to a 100 mL dried, Teflon-lined autoclave and then kept at 200 °C for 24 h. After being cooled to room temperature, the precipitates were collected, washed thoroughly with deionized water and absolute ethanol several times, and then dried in an oven at 60 °C for 12 h. Titanate was then annealed in air at 400 °C for 2 h to obtain Ti^{3+} self-doped TiO_{2-x}. Accordingly to the different volume ratio of TBT to $TiCl_3$, the final products could be denoted as TiO_{2-x}(5-0), TiO_{2-x}(4-1), TiO_{2-x}(3-2), TiO_{2-x}(1-4), and TiO_{2-x}(0-5), respectively.

B. Characterization

The crystalline structures of the prepared samples were measured by X-ray diffraction (DX-2700) (Dandong Hanyuan Instrument, Co., Ltd., Dandong, China). The morphologies of series TiO_{2-x} were examined by a field-emission scanning electron microscope (FE-SEM; Hitachi S4800, Hitachi Corp., Tokyo, Japan) and a transmission electron microscope (TEM; JEM 2100, JEOL Ltd., Tokyo, Japan). X-Ray photoelectron spectroscopy (XPS) measurements were examined on a Kratos AXIS Ultra delay-line detector (DLD; Shimadzu Corp., Tokyo, Japan) (Al K_α monochromatic source). Adventitious C 1*s* peak (284.6 eV) was used as binding energies' reference. The 488 nm laser excited Raman spectra were measured on a quartz sheet equipped with a triple monochromator (TriVista TR557, Princeton Instruments, Trenton, New Jersey) and an argon ion laser (approximately 30 mW on the sample). The charge coupled device (CCD) chip active area covers a wave number of 1089 cm^{-1} and the spectral resolution boasts for 2.5 cm^{-1}. Electron paramagnetic resonance spectroscopy (EPR) was carried out under a xenon lamp. 5 mL 0.5 g/L TiO_2 was mixed with 50 μL 20 mmol/L 5,5-dimethyl-1-pyrroline *N*-oxide (DMPO) for handshaking 5 s. The EPR measurements were started using a Bruker A300 spectrometer (Bruker Corporation, Rheinstetten, Germany). All measurements were performed at a microwave frequency of 9851 MHz and a microwave power of 20 mW. Measurements were done at a center field of 350.8 mT and a sweep field of 10 mT. The field modulation frequency was set to 100 kHz.

C. Photocatalysis experiments

The photocatalytic activities of samples were evaluated by the degradation rate of MB in aqueous under visible light irradiation. The experimental set up placed in a black box consisted of a 200 mL beaker irradiated by a 300 W, 220 V xenon lamp with a 400 nm cutoff filter (CEL-HXUV300, Beijing CEAULIGHT, Beijing, China). The distance between the lamp and the solution is 10 cm. The temperature inside the reactor was maintained at approximately 25 °C by means of a continuous circulation of water surrounding the reactor. In each experiment, 100 mL MB aqueous solution (10 mg/L) was mixed with 50.0 mg photocatalyst powder in the above 200 mL quartz reactor. Before irradiation, the suspension was stirred in the black box for about 30 min till it reached the adsorption–desorption equilibrium. After the photoreaction runs, samples of 4 mL were withdrawn from the suspension at regular time intervals during the irradiation and then centrifuged to separate the photocatalysts. The quantitative determination of remnant MB was conducted by measuring its maximum absorption at 665 nm with a UV-vis spectrometer (Varian Cary 50, Varian Inc., Palo Alto, California).

III. RESULTS AND DISCUSSION

Fig. 1 shows the FE-SEM images of the synthesized Ti^{3+} self-doped TiO_{2-x}. Figure 1(a) illustrates TiO_{2-x}(5-0) with no Ti^{3+} doped that a large quantity of particles have formed with a uniform spindle shape and unique size.

https://doi.org/10.1557/jmr.2017.49 Published online by Cambridge University Press

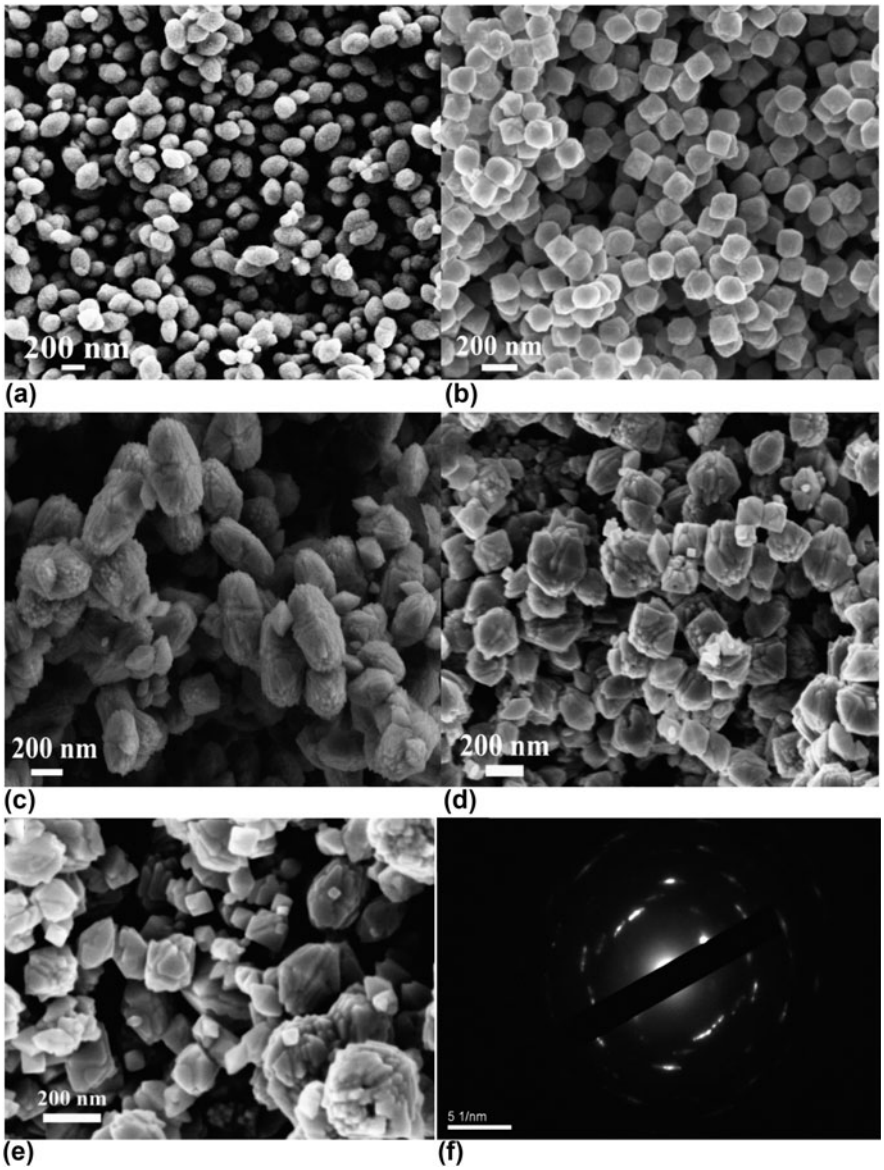


FIG. 1. FE-SEM images of the Ti^{3+} self-doped TiO_{2-x} fabricated with different volume ratios of TBT to $TiCl_3$. (a) TiO_{2-x}(5–0); (b) TiO_{2-x}(4–1); (c) TiO_{2-x}(3–2); (d) TiO_{2-x}(1–4); (e) TiO_{2-x}(0-5); (f) selective area electron diffraction (SAED) of TiO_{2-x}(3–2).

The lengths and diameters are mostly found to be 350–450 nm and 100–200 nm, respectively. These particles were recognized as anatase TiO_2 mesocrystals and have been reported firstly with high visible light photocatalytic activity and extraordinary photocatalytic stability recently.[41] Based on the same strategy, we synthesized the other Ti^{3+} self-doped TiO_{2-x}. TiO_{2-x} (4-1) image is shown in Fig. 1(b), from which we can see that a great deal of uniform tetragonal bipyramids with identical sizes were formed. With the decrease in the ratio of TBT to $TiCl_3$ to 3:2, the catalysis shape of TiO_{2-x}(3-2) changes to capsule-like morphology with a rough surface as is shown in Fig. 1(c). The mean lengths and mean diameters are statistically 540 nm and 325 nm, respectively. There are also some uniform tetragonal bipyramids scarcely scattered among the capsules. With the ratio reaching 1:4, the capsule turns into a round and an irregular size as shown in Fig. 1(d). Extremely when there is no TBT added, the morphology of TiO_{2-x}(0-5) shown in Fig. 1(e) demonstrated that the catalysis is consisted of irregular shapes. The selective area electron diffraction (SAED) of TiO_{2-x}(3-2) [Fig. 1(f)] shows well resolved diffraction spots indicative of a highly crystalline "single-crystal-like" anatase framework. It suggests that the whole assembly of the particle subunits is highly oriented, leading to the formation of the capsule-like particle elongated along the [001] direction. It is clear to see that the diffraction spots are slightly elongated, indicating that a mesocrystal structure was formed.[42,43] The high oriented subunits caused the small lattice

https://doi.org/10.1557/jmr.2017.49 Published online by Cambridge University Press

mismatch between the boundaries of the capsule-like particle when they are assembled in the same orientation.

XRD measurements were carried out to investigate the crystal identity of TiO_2 and the effect of doped Ti^{3+} on the crystal structure of TiO_{2-x}. Figure 2 shows the XRD pattern of TiO_{2-x}. The diffraction peaks at $2\theta = 25.3$, 37.0, 37.8, 38.6, 48.0, 53.1, 55.4, 62.7, 68.8, 70.2, 75.2, and 82.6 correspond to the (101), (103), (004), (112), (200), (105), (211), (204), (116), (220), (215), and (224) planes of anatase TiO_2. All diffraction peaks of the calcined materials in Fig. 3 can be indexed as anatase TiO_2 with standard values in agreement with that of JCPDS card No. 21-1272. The full width at half maximum (FWHM) of the (101) peak at $2\theta = 25.3$ has been measured individually for each sample. The FWHM of (a) to (e) is 0.519, 0.261, 0.267, 0.269, and 0.319 individually. Based on the Scherrer formula, the crystallite sizes of the corresponding TiO_{2-x} could be easily calculated and listed accordingly, 15.5 nm, 30.8 nm, 30.2 nm, 29.9 nm, and 25.2 nm, respectively, from (a) to (e). It is easy to conclude that the crystallite sizes of the corresponding TiO_{2-x} decreases with the decrease of the TBT volume ratio except for sample (a). The large size of spindle-like TiO_2 mesocrystals shown in Fig. 1(a) is composed of many tiny crystallites (12 nm diameter),[41] which is in good coincidence with the XRD determination. Considering the size from SEM shown in Fig. 1 and XRD shown in Fig. 2, we may conclude that all the samples are consisted of tiny crystallites and could be defined as mesocrystals. Judging from the XRD intensity and signal-noise ratio, (b) owns the most excellent crystallinity.

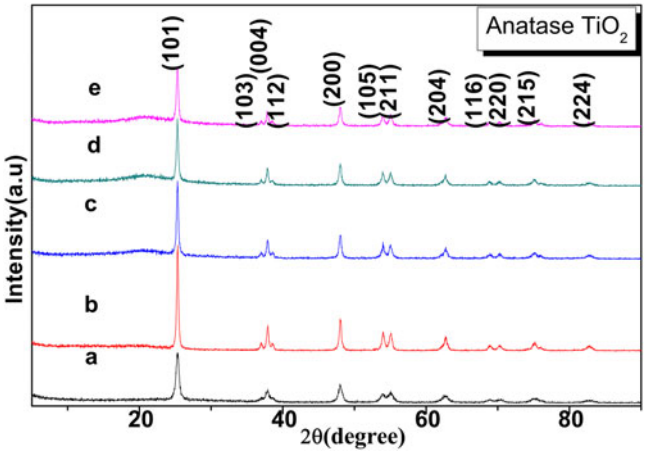


FIG. 2. XRD patterns of Ti^{3+} self-doped TiO_{2-x} fabricated with different volume ratios of TBT to $TiCl_3$. (a) TiO_{2-x}(5-0); (b) TiO_{2-x}(4-1); (c) TiO_{2-x}(3-2); (d) TiO_{2-x}(1-4); (e) TiO_{2-x}(0-5).

To determine the presence of Ti^{3+}, the XPS measurement was conducted as shown in Fig. 3. The measurement was performed over the as-prepared samples of the TiO_{2-x}(3-2) mesocrystal for confirming the surface composition. The Ti 2*p* XPS spectrum is shown in Fig. 3(a), which was composed by two peaks: the Ti $2p_{3/2}$ located at 458.1 eV and the $2p_{1/2}$ located at

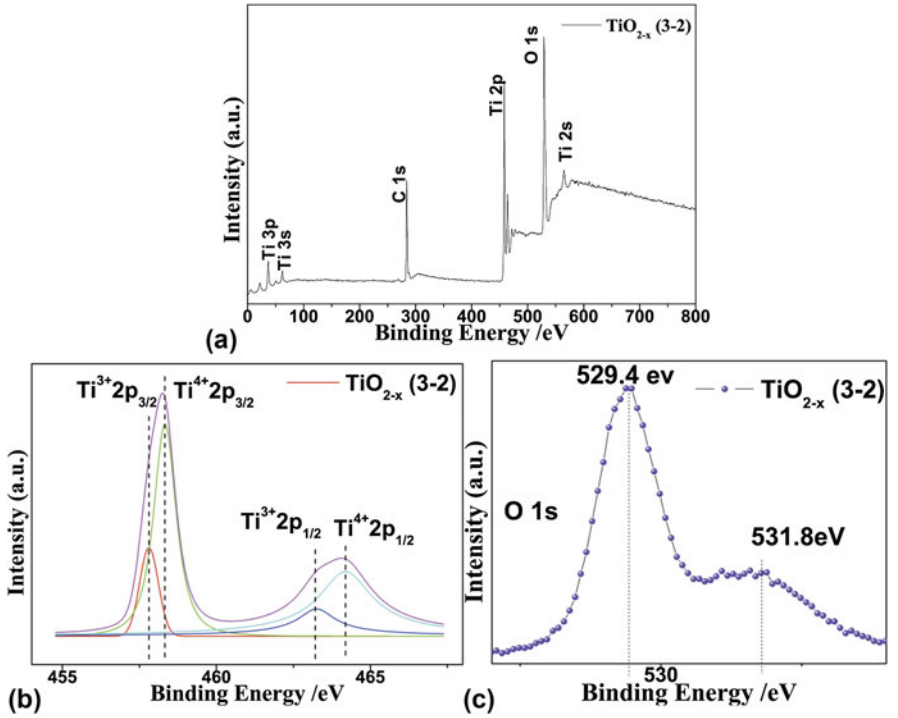


FIG. 3. (a) Wide-scan XPS survey spectra for the TiO_{2-x}(3-2) mesocrystal. (b) Ti 2*p* high-resolution XPS spectra from the TiO_{2-x}(3-2) mesocrystal and (c) O 1*s* high-resolution XPS spectra for the TiO_{2-x}(3-2) mesocrystal.

https://doi.org/10.1557/jmr.2017.49 Published online by Cambridge University Press

463.9 eV. Compared with the literature data of TiO_2, the Ti $2p_{3/2}$ position of TiO_{2-x}(3-2) shifts obviously from 458.7 eV to lower 458.1 eV, indicating multiple oxidation states of the Ti elements. This can be contributed to the different binding energies of Ti^{3+}–O and Ti^{4+}–O. According to the literature,[33,44] the Ti^{3+} species has a lower $2p_{3/2}$ binding energy than Ti^{4+}, and as result, the increasing of the Ti^{3+} contents lead to that the peak of Ti $2p_{3/2}$ shifts to the lower binding energy. Deconvolution of Ti $2p$ XPS data reveals that TiO_{2-x}(3-2) has signals of both Ti^{3+} and Ti^{4+}, appearing at 457.8, 458.3, 463.2, and 464.2 eV, corresponding to Ti^{3+} $2p_{3/2}$, Ti^{4+} $2p_{3/2}$, Ti^{3+} $2p_{1/2}$, and Ti^{4+} $2p_{1/2}$, respectively.[33,44] It should be stressed that the presence of Ti^{3+} is essentially a defective site that captures the hole to prolong the electron hole separation lifetime and suppresses the recombination of electron–hole pairs.

As oxygen vacancies are usually produced with the generation of Ti^{3+} during the preparation process, O 1s XPS spectra were also investigated and shown in Fig. 3. The regions of O 1s XPS spectra are composed of a main peak with a binding energy of 529.4 eV and a minor peak with a binding energy of 531.8 eV. The peaks of 529.4 and 531.8 eV can be attributed to Ti–O in TiO_2 and hydroxyl groups chemisorbed on the surface of the samples, respectively. Normally the O 1s peak of TiO_2 is located at 530.0 eV,[45] but this of TiO_{2-x}(3-2) red shifts to 529.4 eV; this red-shift has also been reported by Gyorgy et al., and they attribute this phenomenon to the oxygen deficiency in TiO_2.[46] The chemisorbed –OH at the binding energy of 531.8 eV is equivalent to surface defects (oxygen vacancies). These defects can act as hole traps to promote electron hole separation, suppress the recombination of electron–hole pairs, and consequently enhance the catalytic activity.[33,44] Meanwhile, the abundant adsorbed –OH on the surface can potentially trap holes to form key oxidative ·OH for advanced oxidation of organic dyes.[33,44]

Raman spectroscopy is a sensitive tool for investigating the changes on the electrons and molecular structure information. To further identify the doped structure and crystallinity of the samples, Raman studies were performed in the range of 120–700 cm^{-1} which is shown in Fig. 4. The Raman peaks at 139.4, 389.0, 508.6, 630.0 cm^{-1} could be assigned to the Raman-active modes of anatase with symmetries E_g (O–Ti–O symmetric stretching), B_{1g} (O–Ti–O wag), A_{1g}, and E_g (O–Ti–O asymmetric stretching), respectively.[41] No characteristic rutile or brookite phase Raman peaks were found, indicating the composition of pure anatase phase TiO_2 mesocrystals. Interesting observations were that the E_g peak at 139.4 cm^{-1} gradually shifted to a lower wave number at 136.5 cm^{-1} as Ti^{3+} doped, and the E_g peak at 630.0 cm^{-1} shifted to the opposite direction at 631.1 cm^{-1}. This indicates that there was an interaction between Ti^{3+} and Ti^{4+}, and the created oxygen vacancies in the lattice structure of the TiO_{2-x} mesocrystal increase with the enhancement of the Ti^{3+} content. Oxygen deficiency can transfer its extra two electrons to the adjacent two Ti^{4+} atoms to form Ti^{3+}, and the presence of the oxygen vacancies lead to the change of atomic coordination numbers and bonding length of the Ti–O–Ti network in the Ti^{3+} self-doped TiO_{2-x} mesocrystal. Therefore, it is not strange to see that the O–Ti–O stretching frequency shifted with increase in the Ti^{3+}/TBT molar ratio. The oxygen vacancies can act as traps to capture photoelectrons, which make a contribution to inhibit the charge recombination. Thus, the XRD and Raman characterization of the TiO_{2-x} mesocrystal demonstrate the high crystallinity of titania materials and the presence of the anatase phase.

The nitrogen adsorption–desorption isotherms were carried out to characterize the specific surface area (S_{BET}) and pore structure of the photocatalysts. According to the isotherms shown in Fig. 5, the isotherms for the P25 and TiO_{2-x}(3-2) mesocrystal could be identified as type IV (IUPAC classification), which was a characteristic of mesoporous materials, while the isotherms for the TiO_{2-x} (5-0) mesocrystal could be identified as type I, which was a characteristic of porous materials exhibiting a narrow distribution of relatively uniform (cylindrical-like) pores. In addition, the hysteresis loop resemble H3 in the IUPAC classification, indicating that the P25 and TiO_{2-x}(3-2) mesocrystal comprised aggregates of nanorods (loose assemblages) exhibiting a narrow distribution of relatively uniform slit-like pores. The Brunauer–Emmett–Teller (BET) specific surface area is 73.7 m^2/g, 52.6 m^2/g, and 13.6 m^2/g, respectively, for TiO_{2-x}(5-0), P25, and TiO_{2-x}(3-2).

The fluorescence spectrum of Ti^{3+} self-doped nanoparticles presents a blue shift relatively to the spectra of P25 (Fig. 6). And the fluorescence intensity is enhanced

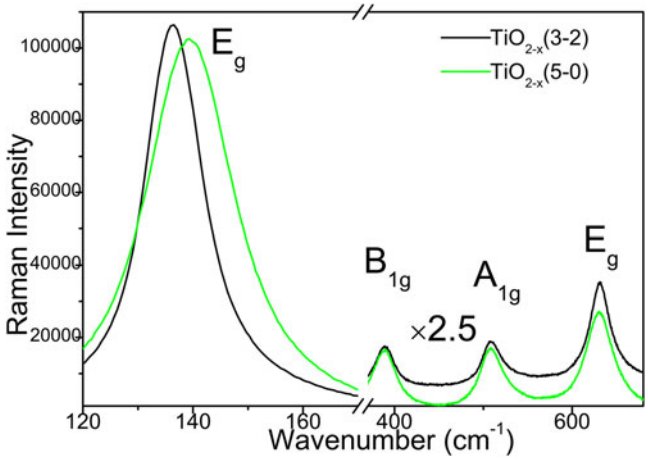


FIG. 4. Raman spectra of the TiO_{2-x}(3-2) mesocrystal and TiO_{2-x}(5-0) mesocrystal.

https://doi.org/10.1557/jmr.2017.49 Published online by Cambridge University Press

after Ti^{3+} is doped to TiO_2 composites. The emission wave length were 485 nm, 485 nm, 586 nm for the TiO_{2-x}(3-2) mesocrystal, TiO_{2-x}(5-0) mesocrystal, and P25, respectively. Obviously, the Ti^{3+} self-doping process greatly changed the crystal structure and the semiconductor energy band structure of TiO_2 nanoparticles.

Figure 7 shows the fluorescence decay profile of the P25, TiO_{2-x}(3-2) mesocrystal, and TiO_{2-x}(5-0) mesocrystal. Their decay lifetime can be obtained by using exponential function fitting. We observed that the relaxation lifetime of photo-generated electrons in the P25 is about 23.85 ns, while that in the TiO_{2-x}(3-2) mesocrystal and TiO_{2-x}(5-0) mesocrystal is 5.20 and 4.61 ns, respectively, one in five of P25.

Light response properties were studied by UV–vis spectroscopy and the effect of Ti^{3+} doping content on UV–vis absorption property is revealed in Fig. 8. It shows that the absorption of blank P25 and TiO_{2-x}(5-0) mesocrystal is only located at the ultraviolet (UV) region below 390 nm, whereas the absorption edge of TiO_{2-x}(3-2) composites shows redshift to near 420 nm. The presence of Ti^{3+} narrowed the band gap. The pronounced low-energy absorption band at 420 nm is in good agreement with the reported values of Ti^{3+} self-doped nanoparticles.

An EPR spin trapping study was conducted to verify the presence of radicals and identify radical species which may be responsible for the degradation of MB. The EPR spectra of the Ti^{3+}–TiO_{2-x} sample, $MesoTiO_2$ sample, and P25 sample dispersed in water under UV irradiation are shown in Fig. 9 and the ESR spectra of the sample dispersed in methanol are shown in Fig. 10. The spectra (Fig. 9) showed a four-line EPR characteristic signal, with Hamiltonian parameters characterized by the hyperfine splitting for the 1:2:2:1 signal $a_N = a_H = 1.48$ mT, which are typical for the ·DMPO-OH adduct.[47] Furthermore, the ESR spectra intensity of TiO_{2-x}(3-2) was a little stronger than other two.

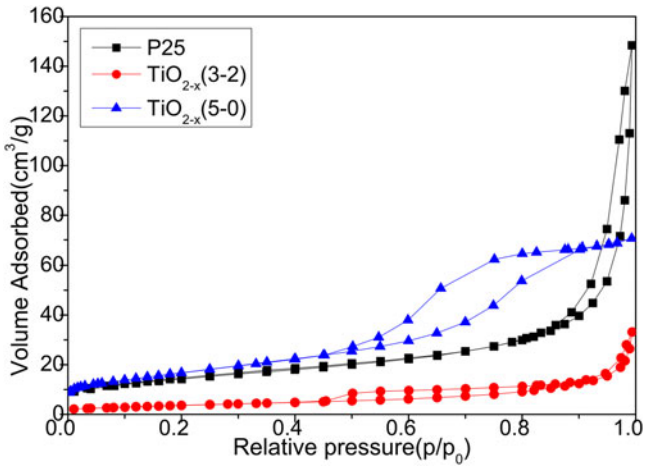


FIG. 5. N_2 adsorption–desorption isotherms of the P25, TiO_{2-x}(3-2) mesocrystal, and TiO_{2-x}(5-0) mesocrystal.

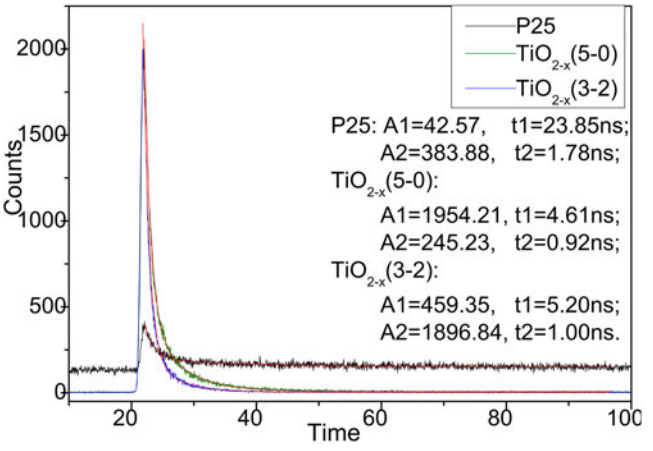


FIG. 7. Fluorescence decay profile of the P25, TiO_{2-x}(3-2) mesocrystal, and TiO_{2-x}(5-0) mesocrystal dispersed in MeCN and their exponential function fitting data are shown in the figure.

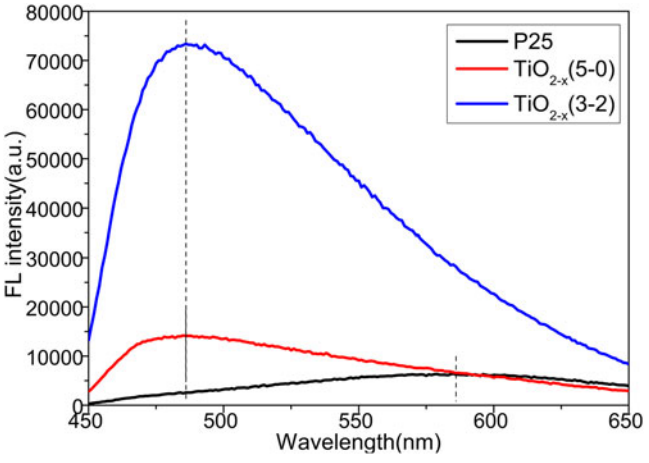


FIG. 6. Fluorescence spectra of the P25, TiO_{2-x}(3-2) mesocrystal, and TiO_{2-x}(5-0) mesocrystal.

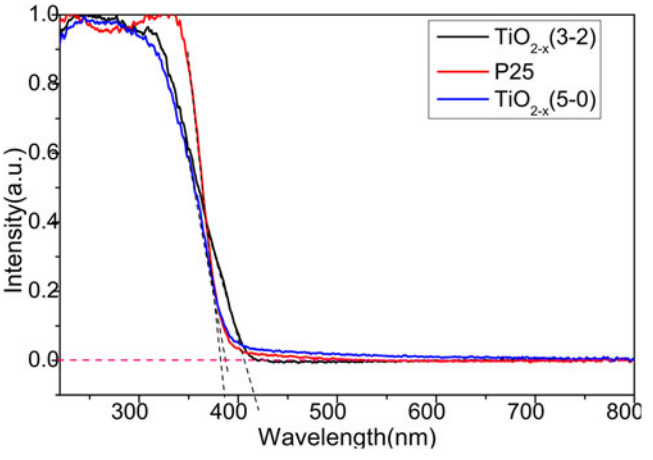


FIG. 8. UV–vis absorption spectra of the TiO_{2-x}(3-2) mesocrystal and TiO_{2-x}(5-0) mesocrystal composites, UV–vis absorption spectra of P25 also included for comparison.

https://doi.org/10.1557/jmr.2017.49 Published online by Cambridge University Press

The EPR spectra, monitored upon continuous irradiation of TiO_2 suspensions dispersed in methanol (Fig. 10), demonstrate the formation of ·DMPO-OH simultaneously with a further six-line paramagnetic signal characterized by the hyperfine splitting $a_N = 0.790$ mT, $a_H\ \beta = 1.12$ mT and $a_H\ \gamma\ (2H) = 0.480$ mT, which are typical for the DMPO oxidation product 5,5-dimethyl-1-pyrrolidone-2-oxyl (·DMPO-X, i.e., O_2^{-}/·OOH[48]).

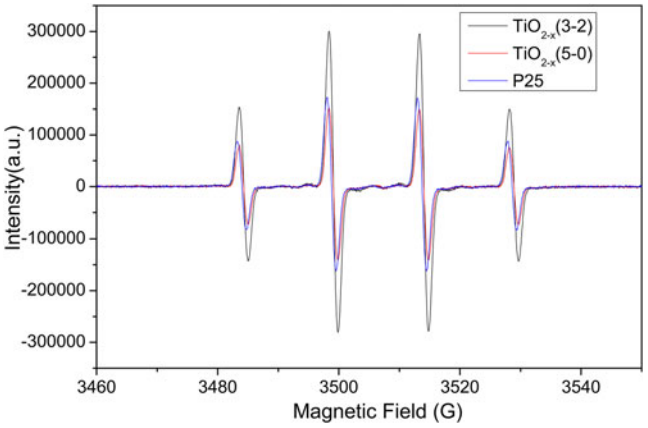


FIG. 9. EPR spectra measured upon continuous irradiation of aqueous suspensions in the presence of DMPO (2 mmol/L) at TiO_{2-x}(3-2) mesocrystal, TiO_{2-x}(5-0) mesocrystal, and P25.

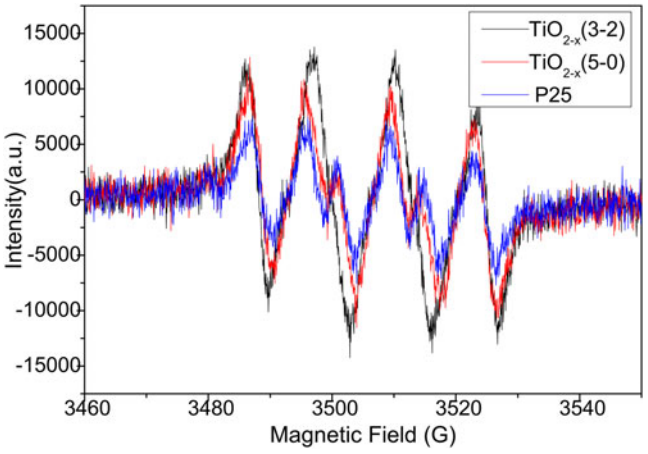
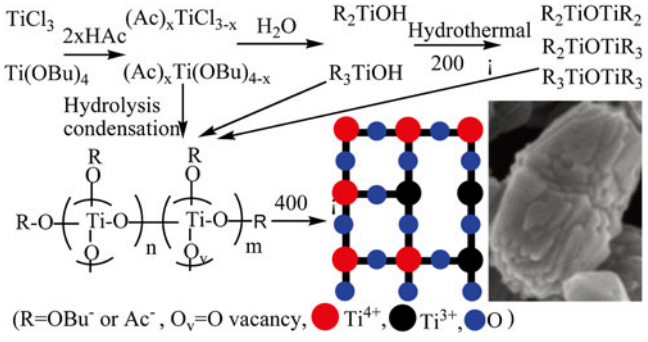


FIG. 10. EPR spectra measured upon continuous irradiation of oxygen-saturated methanol suspensions in the presence of DMPO (2 mmol/L) at TiO_{2-x}(3-2) mesocrystal, TiO_{2-x}(5-0) mesocrystal, and P25.



SCHEME 1. Schematic illustration of a tentative mechanism for the formation of the Ti^{3+} self-doped TiO_{2-x} mesocrystal.

Based on the above results, a tentative mechanism is proposed, as illustrated in Scheme 1, to interpret the formation of the Ti^{3+} self-doped TiO_{2-x} mesocrystal.

$TiCl_3$ and $Ti(OBu)_4$ are the most reactive species and easy to be hydrolyzed or coordinated with HAc. In the current solvothermal conditions at 200 °C, the coordination complexes $(Ac)_xTi(OBu)_{4-x}$, $(Ac)_xTiCl_{3-x}$ and hydrolysate R_2TiOH, R_3OH are unstable and easy to poly-condense. Subsequently, Ti–O–Ti bonds would form by co-polycondensation processes, leading to the formation of the Ti^{4+} and Ti^{3+} block copolymers. With the condensation processes continuing, the large copolymers crystallized and heated to break down gradually to release soluble nucleation species for the growth of anatase nanocrystals in the solution.

The anatase nanocrystals grew along one prevailing direction, together with minor attachment along some side facets, resulting in the formation of the anisotropic developed anatase mesocrystals elongated along the prevailing direction. With the increase of the Ti^{3+} content, the side facets' attachment becomes equal with the main facet nanocrystals' growth, resulting in round sphere morphology. It is well known that fast hydrolysis and condensation rate lead to the precipitation of amorphous TiO_2; in our experiment acetic acids were used both as a stabilizing solvent and as a chemical modifier of titanium alkoxides to lower the reactivity of the precursors. Finally, 400 °C calcination subsequently removed the organic residuals and increased the nanocrystal size of anatase Ti^{3+} self-doped TiO_{2-x} mesocrystals.

The photocatalytic degradation of MB in the aqueous phase was selected as the probe reaction to evaluate the photocatalytic activity of the Ti^{3+} self-doped TiO_{2-x} mesocrystal. For comparison, the photocatalytic activity of every sample was tested under identical conditions. The change of MB concentration as a function of illumination time was shown in Figs. 11(A) and 11(B). Five different ratio samples (a, b, c, d, and e) showed 57%, 70%, 74%, 72, and 69% decolorization rates ($1 - C/C_0$), respectively, under xenon lamp illumination after 180 min. It can be seen that the TiO_{2-x}(5-0) mesocrystal displays the lowest photocatalytic degradation rate under visible light irradiation due to its wide band gap, whereas, the TiO_{2-x} mesocrystal with different Ti^{3+} doped contents demonstrated higher photodegradation efficiency. Through careful observation, the catalytic efficiency increased with Ti^{3+} doped, reached 74% utmost over the TiO_{2-x}(3-2) mesocrystal, and then decreased with the further increase ratio of Ti^{3+} doping in the TiO_{2-x} nanocomposite; the photocatalytic activity of the TiO_{2-x}(3-2) mesocrystal

https://doi.org/10.1557/jmr.2017.49 Published online by Cambridge University Press

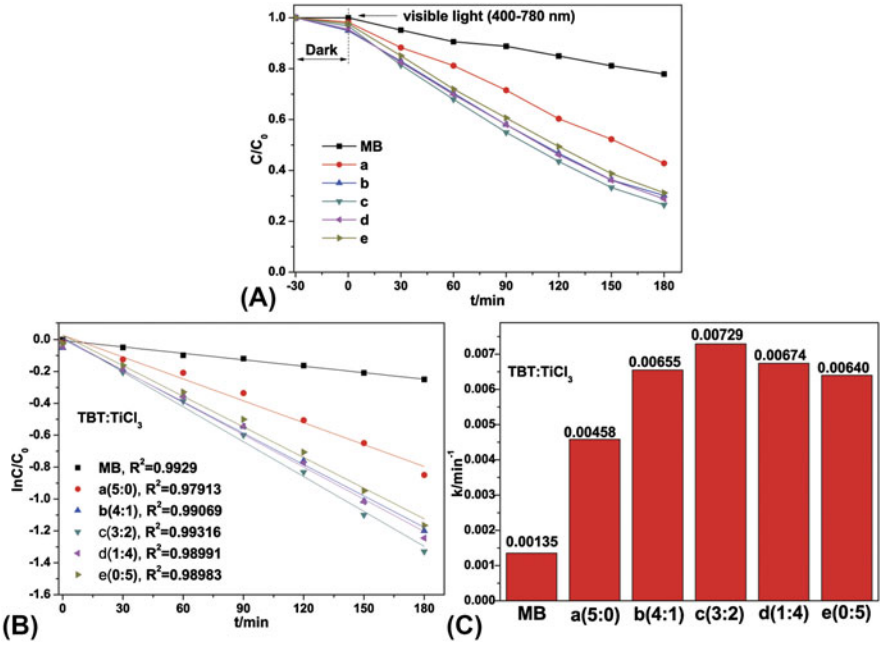


FIG. 11. (A) Photodegradation of MB upon visible light irradiation over the TiO_{2-x} mesocrystal fabricated with different volume ratios of TBT to $TiCl_3$. (a) TiO_{2-x}(5-0); (b) TiO_{2-x}(4-1); (c) TiO_{2-x}(3-2); (d) TiO_{2-x}(1-4); (e) TiO_{2-x}(0-5). (B) Kinetic linear fitting curves for the photocatalytic degradation of MB over the TiO_{2-x} mesocrystal with different volume ratios under visible light irradiation. (C) Value of the rate constant k of the photodegradation of MB over the TiO_{2-x} mesocrystal with different volume ratios.

shows the highest photocatalytic activity for the degradation of MB. On the basis of a simplified Langmuir–Hinshelwood model, the linear relationship of $\ln(C/C_0)$ versus time [see Fig. 11(B)] upon visible light irradiation indicates that MB degradation follows a pseudo first order kinetic, and the apparent rate constant (k) shown in Fig. 11(C) was calculated from the plot of $\ln(C/C_0)$ versus time. The highest apparent rate constant, obtained for the TiO_{2-x} (3-2) mesocrystal, is 7.29×10^{-3} min^{-1}, which shows 1.59, 1.11, 1.08, and 1.14-fold photocatalytic activity improvement over the TiO_{2-x}(5-0), TiO_{2-x}(4-1), TiO_{2-x} (1-4), and TiO_{2-x}(0–5) mesocrystals, respectively. The high efficiency performance could be ascribed to its unique doping structure and low band gap energy.

Durability test was performed to confirm the photocatalytic stability of the synthesized TiO_{2-x}(3-2) mesocrystal, which was very important for the practical application. According to Fig. 12, the 10 mg/L MB was 75% degradated in 180 min for all the recycles for dye sensitized TiO_2, keeping stable the catalysis performance with the original first run of TiO_{2-x}(3-2) nanoparticles as shown in Fig. 11. The MB photodegradation efficiency changed a little after 6 recycles of the experiment under identical conditions, indicating that the photocatalyst has superior photocatalytic stability.

The incorporation of Ti^{3+} in the TiO_{2-x} mesocrystal ameliorates the hydrophilic compatibility, which is significant for photocatalysis and super hydrophilic effects. However, theoretical work showed that for achieving

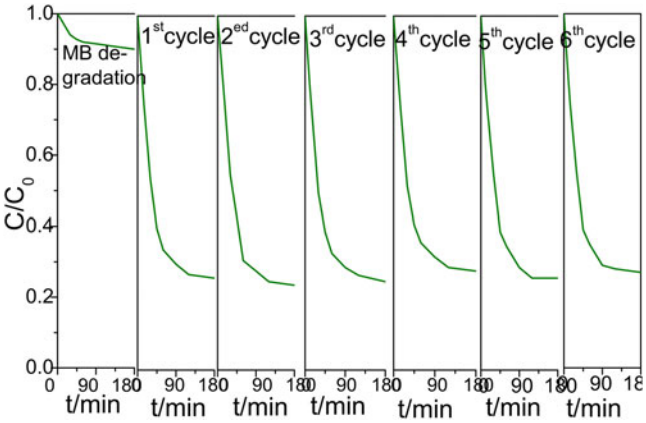


FIG. 12. Stability study over TiO_{2-x}(3-2) for MB photodegradation under visible light irradiation.

high efficiency visible light activity, the Ti^{3+} doping concentration must be kept high enough to create large amounts of lattice disorder that could induce a continuous vacancy band of mid-gap electronic states which is largely (0.75–1.18 eV) below the conduction band (CB) edge of TiO_2. Otherwise, a low Ti^{3+} doping concentration only produces localized single oxygen defect that actually deteriorates the electron mobility and exhibits a negligible visible photoactivity, or even worse to act as electron–hole pair recombination sites. The electronic transitions from mid-gap electronic states to CB, and from valent band (VB) to mid-gap electronic states, are

https://doi.org/10.1557/jmr.2017.49 Published online by Cambridge University Press

responsible for the TiO_{2-x} mesocrystal visible light activity. Furthermore the mid-gap states may trap the photo-generated electrons, prolong its lifetime, and enhance its transfer possibility to react with O_2 adsorbed on the surface of TiO_2. Therefore, the presence of appropriate amount of Ti^{3+} states in TiO_2 results in the reduction of the electron–hole pair recombination rate and enhances visible light photocatalytic activity.[21] However when the dopant concentration becomes too high ($TiCl_3$ to TBT molar ratio of higher than 2:3), the recombination rate will increase because the distance between trapping sites in a particle decreases with the number of dopants.[21] This discussion and theoretical explanation is account for our experimental visible light excited photocatalytic activity.

IV. CONCLUSION

In summary, a unique one-pot solvothermal method is used to prepare different Ti^{3+} content doped TiO_{2-x} mesocrystals. Morphology varies from uniform spindle shape and tetragonal bipyramid to capsule-like shapes which can be tailored easily by tuning the precursor ratio of $TiCl_3$ to TBT. SEM and XRD demonstrate that the catalysts produced in this method consist of tiny crystallites and could be classified as mesocrystals. The resulting Ti^{3+} self-doped TiO_{2-x} mesocrystals show enhanced visible light-driven photocatalytic oxidation on MB, which is attributed to the presence of oxygen vacancies and Ti^{3+} species. TiO_{2-x}(3-2) mesocrystals show the highest photocatalytic activity. This study demonstrates a simple and cost-efficient approach to narrow the band gap of TiO_2 and develops a new effective method to prepare Ti^{3+} self-doped TiO_{2-x} mesocrystals with high photocatalysis performance under visible light irradiation.

ACKNOWLEDGMENTS

This work was supported by grants from the National Natural Science Foundation of China (No. 21271155 and 21473161), Zhejiang Provincial Natural Science Foundation of China (LZ17B030001), Zhejiang Provincial Top Key Academic Discipline of Chemical Engineering and Technology, Alexander von Humboldt Foundation (No. 1141172), and Zhejiang SCI-TECH University for 521 distinguished scholar's scheme.

REFERENCES

1. A. Fujishima and K. Honda: Electrochemical photolysis of water at a semiconductor electrode. *Nature* **238**(5358), 37 (1972).
2. M.R. Hoffmann, S.T. Martin, W.Y. Choi, and D.W. Bahnemann: Environmental applications of semiconductor photocatalysis. *Chem. Rev.* **95**, 69 (1995).
3. S.G. Kumar and L.G. Devi: Review on modified TiO_2 photocatalysis under UV/visible Light: Selected results and related mechanisms on interfacial charge carrier transfer dynamics. *J. Phys. Chem. A* **115**, 13211 (2011).
4. X. Li, J. Yu, and M. Jaroniec: Hierarchical photocatalysts. *Chem. Soc. Rev.* **45**, 2603 (2016).
5. X. Li, J. Yu, J. Low, Y. Fang, J. Xiao, and X. Chen: Engineering heterogeneous semiconductors for solar water splitting. *J. Mater. Chem. A* **3**, 2485 (2015).
6. E.M. Samsudin, S.B.A. Hamid, J.C. Juan, W.J. Basirun, and A.E. Kandjani: Surface modification of mixed-phase hydrogenated TiO_2 and corresponding photocatalytic response. *Appl. Surf. Sci.* **359**, 883 (2015).
7. W.J. Ong, L.L. Tan, S.P. Chai, S.T. Yong, and A.R. Mohamed: Highly reactive {001} facets of TiO_2-based composites: Synthesis, formation mechanism and characterization. *Nanoscale* **6**, 1946 (2014).
8. J. Seo, J.H. Noh, and S.I. Seok: Rational strategies for efficient perovskite solar cells. *Acc. Chem. Res.* **49**, 562 (2016).
9. S.N.R. Inturi, T. Boningari, M. Suidan, and P.G. Smirniotis: Visible-light-induced photodegradation of gas phase acetonitrile using aerosol-made transition metal (V, Cr, Fe, Co, Mn, Mo, Ni, Cu, Y, Ce, and Zr) doped TiO_2. *Appl. Catal., B* **144**, 333 (2014).
10. W.Y. Choi, A. Termin, and M.R. Hoffmann: The role of metal-ion dopants in quantum-sized TiO_2-correlation between photoreactivity and charge-carrier recombination dynamics. *J. Phys. Chem.* **98**, 13669 (1994).
11. S.Z. Khalajabadi, M.R.A. Kadir, S. Izman, and M.Z.M. Yusop: Facile fabrication of hydrophobic surfaces on mechanically alloyed-Mg/HA/TiO_2/MgO bionanocomposites. *Appl. Surf. Sci.* **324**, 380 (2015).
12. X. Li, T. Xia, C. Xu, J. Murowchick, and X. Chen: Synthesis and photoactivity of nanostructured CdS-TiO_2 composite catalysts. *Catal. Today* **225**, 64 (2014).
13. A.E. Giannakas, M. Antonopoulou, C. Daikopoulos, Y. Deligiannakis, and I. Konstantinou: Characterization and catalytic performance of B-doped, B-N co-doped and B-N-F tri-doped TiO_2 towards simultaneous Cr(VI) reduction and benzoic acid oxidation. *Appl. Catal., B* **184**, 44 (2016).
14. R. Jaiswal, N. Patel, A. Dashora, R. Fernandes, M. Yadav, R. Edla, R.S. Varma, D.C. Kothari, B.L. Ahuja, and A. Miotello: Efficient Co-B-codoped TiO_2 photocatalyst for degradation of organic water pollutant under visible light. *Appl. Catal., B* **183**, 242 (2016).
15. J.H. Park, S. Kim, and A.J. Bard: Novel carbon-doped TiO_2 nanotube arrays with high aspect ratios for efficient solar water splitting. *Nano Lett.* **6**, 24 (2006).
16. S. Banerjee, D.D. Dionysiou, and S.C. Pillai: Self-cleaning applications of TiO_2 by photo-induced hydrophilicity and photocatalysis. *Appl. Catal., B* **176**, 396 (2015).
17. S. Ivanov, A. Barylyak, K. Besaha, A. Bund, Y. Bobitski, R. Wojnarowska-Nowak, I. Yaremchuk, and M. Kus-Liskiewicz: Synthesis, characterization, and photocatalytic properties of sulfur- and carbon-codoped TiO_2 nanoparticles. *Nanoscale Res. Lett.* **11**, 140 (2016).
18. P. Zhang, M. Fujitsuka, and T. Majima: TiO_2 mesocrystal with nitrogen and fluorine codoping during topochemical transformation: Efficient visible light induced photocatalyst with the codopants. *Appl. Catal., B* **185**, 181 (2016).
19. Y. Zhang, M. Creatore, Q-B. Ma, A. El Boukili, L. Gao, M.A. Verheijen, M.W.G.M. Verhoeven, and E.J.M. Hensen: Nitrogen-doping of bulk and nanotubular TiO_2 photocatalysts by plasma-assisted atomic layer deposition. *Appl. Surf. Sci.* **330**, 476 (2015).
20. D. Qu, M. Zheng, P. Du, Y. Zhou, L.G. Zhang, D. Li, H.Q. Tan, Z. Zhao, Z.G. Xie, and Z.C. Sun: Highly luminescent S, N co-doped graphene quantum dots with broad visible absorption bands for visible light photocatalysts. *Nanoscale* **5**, 12272 (2013).
21. J.C. Yu, J.G. Yu, W.K. Ho, Z.T. Jiang, and L.Z. Zhang: Effects of F-doping on the photocatalytic activity and microstructures of nanocrystalline TiO_2 powders. *Chem. Mater.* **14**, 3808 (2002).

https://doi.org/10.1557/jmr.2017.49 Published online by Cambridge University Press

22. O. Elbanna, P. Zhang, M. Fujitsuka, and T. Majima: Facile preparation of nitrogen and fluorine codoped TiO_2 mesocrystal with visible light photocatalytic activity. *Appl. Catal., B* **192**, 80 (2016).
23. E.M. Samsudin, S.B. Abd Hamid, J.C. Juan, W.J. Basirun, and G. Centi: Synergetic effects in novel hydrogenated F-doped TiO_2 photocatalysts. *Appl. Surf. Sci.* **370**, 380 (2016).
24. X.B. Chen, L. Liu, P.Y. Yu, and S.S. Mao: Increasing solar absorption for photocatalysis with black hydrogenated titanium dioxide nanocrystals. *Science* **331**, 746 (2011).
25. K. Li, S.M. Gao, Q.Y. Wang, H. Xu, Z.Y. Wang, B.B. Huang, Y. Dai, and J. Lu: *In situ* reduced synthesis of Ti^{3+} self-doped TiO_2/g-C_3N_4 heterojunctions with high photocatalytic performance under LED light irradiation. *ACS Appl. Mater. Interfaces* **7**, 9023 (2015).
26. Z.Q. Wang, B. Wen, Q.Q. Hao, L.M. Liu, C.Y. Zhou, X.C. Mao, X.F. Lang, W.J. Yin, D.X. Dai, A. Selloni, and X.M. Yang: Localized excitation of Ti^{3+} ions in the photoabsorption and photocatalytic activity of reduced rutile TiO_2. *J. Am. Chem. Soc.* **137**, 9146 (2015).
27. Y. Chen, W.Z. Li, J.Y. Wang, Y.L. Gan, L. Liu, and M.T. Ju: Microwave-assisted ionic liquid synthesis of Ti^{3+} self-doped TiO_2 hollow nanocrystals with enhanced visible-light photoactivity. *Appl. Catal., B* **191**, 94 (2016).
28. X. Chen, L. Liu, and F. Huang: Black titanium dioxide (TiO_2) nanomaterials. *Chem. Soc. Rev.* **44**, 1861 (2015).
29. L. Liu and X. Chen: Titanium dioxide nanomaterials: Self-structural modifications. *Chem. Rev.* **114**, 9890 (2014).
30. D. Lu, G. Zhang, and Z. Wan: Visible-light-driven g-C_3N_4/Ti^{3+}–TiO_2 photocatalyst co-exposed {001} and {101} facets and its enhanced photocatalytic activities for organic pollutant degradation and Cr(VI) reduction. *Appl. Surf. Sci.* **358**, 223 (2015).
31. J. Tian, X. Hu, H. Yang, Y. Zhou, H. Cui, and H. Liu: High yield production of reduced TiO_2 with enhanced photocatalytic activity. *Appl. Surf. Sci.* **360**, 738 (2016).
32. J. Wang, P. Yang, and B. Huang: Self-doped TiO_{2-x} nanowires with enhanced photocatalytic activity: Facile synthesis and effects of the Ti^{3+}. *Appl. Surf. Sci.* **356**, 391 (2015).
33. X. Liu, H. Xu, L.R. Grabstanowicz, S.M. Gao, Z.Z. Lou, W.J. Wang, B.B. Huang, Y. Dai, and T. Xu: Ti^{3+} self-doped TiO_{2-x} anatase nanoparticles via oxidation of TiH_2 in H_2O_2. *Catal. Today* **225**, 80 (2014).
34. A. Ali, I. Ruzybayev, E. Yassitepe, A. Karim, S.I. Shah, and A.S. Bhatti: Phase transformations in the pulsed laser deposition grown TiO_2 thin films as a consequence of O-2 partial pressure and Nd doping. *J. Phys. Chem. C* **119**, 11578 (2015).
35. X. Chen, D.X. Zhao, K.W. Liu, C.R. Wang, L. Liu, B.H. Li, Z.Z. Zhang, and D.Z. Shen: Laser-modified black titanium oxide nanospheres and their photocatalytic activities under visible light. *ACS Appl. Mater. Interfaces* **7**, 16070 (2015).
36. L.Q. Wang, D.R. Baer, and M.H. Engelhard: Creation of variable concentrations of defects on TiO_2(110) using low-density electron-beams. *Surf. Sci.* **320**, 295 (1994).
37. X.M. Zhou, N. Liu, and P. Schmuki: Ar^+-ion bombardment of TiO_2 nanotubes creates co-catalytic effect for photocatalytic open circuit hydrogen evolution. *Electrochem. Commun.* **49**, 60 (2014).
38. C. Di Valentin, G. Pacchioni, and A. Selloni: Reduced and n-type doped TiO_2: Nature of Ti^{3+} species. *J. Phys. Chem. C* **113**, 20543 (2009).
39. I. Justicia, P. Ordejon, G. Canto, J.L. Mozos, J. Fraxedas, G.A. Battiston, R. Gerbasi, and A. Figueras: Designed self-doped titanium oxide thin films for efficient visible-light photocatalysis. *Adv. Mater.* **14**, 1399 (2002).
40. H. Colfen and M. Antonietti: Mesocrystals: Inorganic superstructures made by highly parallel crystallization and controlled alignment. *Angew. Chem., Int. Ed.* **44**, 5576 (2005).
41. T.H. Han, H.G. Wang, and X.M. Zheng: Gold nanoparticle incorporation into nanoporous anatase TiO_2 mesocrystal using a simple deposition-precipitation method for photocatalytic applications. *RSC Adv.* **6**, 7829 (2016).
42. F.F. Chen, F.L. Cao, H.X. Li, and Z.F. Bian: Exploring the important role of nanocrystals orientation in TiO_2 superstructure on photocatalytic performances. *Langmuir* **31**, 3494 (2015).
43. Z.S. Hong, M.D. Wei, T.B. Lan, L.L. Jiang, and G.Z. Cao: Additive-free synthesis of unique TiO_2 mesocrystals with enhanced lithium-ion intercalation properties. *Energy Environ. Sci.* **5**, 5408 (2012).
44. T.S. Yang, M.C. Yang, C.B. Shiu, W.K. Chang, and M.S. Wong: Effect of N-2 ion flux on the photocatalysis of nitrogen-doped titanium oxide films by electron-beam evaporation. *Appl. Surf. Sci.* **252**, 3729 (2006).
45. A.F. Carley, P.R. Chalker, J.C. Riviere, and M.W. Roberts: The identification and characterisation of mixed oxidation states at oxidised titanium surfaces by analysis of X-ray photoelectron spectra. *J. Chem. Soc., Faraday Trans. 1* **83**, 351 (1987).
46. E. György, A. Pérez del Pino, P. Serra, and J.L. Morenza: Depth profiling characterisation of the surface layer obtained by pulsed Nd:YAG laser irradiation of titanium in nitrogen. *Surf. Coat. Technol.* **173**, 265 (2003).
47. J.M. Fontmorin, R.C.B. Castillo, W.Z. Tang, and M. Sillanpaa: Stability of 5,5-dimethyl-1-pyrroline-*N*-oxide as a spin-trap for quantification of hydroxyl radicals in processes based on Fenton reaction. *Water Res.* **99**, 24 (2016).
48. A.S.W. Li, K.B. Cummings, H.P. Rothling, G.R. Buettner, and C.F. Chignell: A spin-trapping database implemented on the IBM PC/AT. *J. Magn. Reson.* **79**, 140 (1988).

https://doi.org/10.1557/jmr.2017.49 Published online by Cambridge University Press